1-D Reconfigurable Pseudo-Doherty Load Modulated Balanced Amplifier With Intrinsic VSWR Resilience Across Wide Bandwidth

Jiachen Guo, *Student Member, IEEE*, Yuchen Cao, *Member, IEEE*, and Kenle Chen, *Senior Member, IEEE*

***Abstract*— This article presents the first-ever wideband pseudo-Doherty load-modulated balanced amplifier (PD-LMBA) with load-mismatch tolerance through 1-D reconfiguration. It is theoretically unveiled that when the control amplifier (CA, as a carrier) in PD-LMBA is driven to its saturation, it is endowed with a duality between the current source (CS) and voltage source (VS), which makes the BA (as peaking) have complementary load-modulation trajectories for the two sub-amplifiers (BA1 and BA2) under load mismatch. As a result, the BA in PD-LMBA inherits the intrinsic load insensitivity from the generic quadrature-balanced amplifier. Meanwhile, the saturation power of CA can be maintained by only reconfiguring the dc bias voltage ($V_{DD,CA}$) that solely depends on the real part of load impedance, real(Z_L). As such, the degree of freedom for PA reconfiguration and load sensing (ideally) is minimized to 1-D, and the entire PD-LMBA can maintain a nearly constant efficiency profile against arbitrary load mismatch. The theoretical analysis is well verified using emulated circuit model, and it is further experimentally validated by a prototype designed with GaN transistors and wideband quadrature hybrids. As a proof of concept, the fabricated PD-LMBA circuit achieves state-of-the-art performance in measurement at matched load with 1.7–2.9 GHz of bandwidth, 65%–77% of drain efficiency at peak power of 39–43 dBm, and 55%–71% of efficiency at 10-dB output back-off (OBO). More importantly, the prototype also experimentally exhibits excellent mismatch resilience through 1-D reconfiguration, which is demonstrated at three representative in-band frequencies of 1.7, 2.1 and 2.5 GHz at 2:1 VSWR. Specifically, a maximum drain efficiency from 51.9% to 72.8% at peak power is achieved over the entire 2:1 VSWR circle, and an efficiency up to 65.4% is measured at 10-dB back-off. Modulated evaluation using an LTE signal is also performed, in which the 1-D reconfigurable PD-LMBA exhibits an excellent average efficiency at load mismatch that aggressively outperforms the state-of-the-art.**

***Index Terms*— Balanced amplifier, Doherty power amplifier (PA), linearity, load mismatch, reconfigurable.**

Manuscript received 13 September 2022; revised 16 November 2022; accepted 22 December 2022. Date of publication 31 January 2023; date of current version 5 June 2023. This work was supported in part by the National Science Foundation under Award 2218808. *(Corresponding author: Jiachen Guo.)*

Jiachen Guo and Kenle Chen are with the Department of Electrical and Computer Engineering, University of Central Florida, Orlando, FL 32816 USA (e-mail: jiachen@knights.ucf.edu; kenle.chen@ucf.edu).

Yuchen Cao was with the Department of Electrical and Computer Engineering, University of Central Florida, Orlando, FL 32816 USA. He is now with Qorvo, Inc., Apopka, FL 32703 USA (e-mail: yuchencao@knights.ucf.edu).

Color versions of one or more figures in this article are available at https://doi.org/10.1109/TMTT.2023.3239399.

Digital Object Identifier 10.1109/TMTT.2023.3239399

I. Introduction

SPECTRALLY efficient high-data-rate modulations have been widely adopted in emerging communications standards to meet the ever-growing demand for high-speed wireless data transmission. However, these advanced modulation schemes greatly increase the peak-to-average power ratio (PAPR) of signals due to a large number of sub-carriers and higher-order digital mapping (e.g., 4096QAM). Efficient amplification of such high-PAPR signals requires enhanced efficiency of power amplifiers (PAs) over a large output back-off (OBO) range. Moreover, with the evolution of the wireless standard and the expansion of spectrum into higher frequencies (e.g., 3–5-GHz frequency range newly allocated to 5G), the PAs need to cover wider bandwidth and support multimode or multiband operations, thus making the system sustainable in complexity and cost. Consequently, enhanced back-off efficiency range and broad bandwidth gradually become crucial targets for exploiting high-efficiency PAs. Besides the legacy technologies of envelope tracking (ET) [1] and Doherty PA [2], [3], [4], many new architectures and techniques [5], [6] have been proposed recently, e.g., load-modulated balanced amplifiers [7], [8], [9], [10], [11], [12], [13], [14], [15], [16], [17], [18], offering unprecedented efficiency, OBO range, and bandwidth.

Meanwhile, massive MIMO has been a key signature of 5G systems for enhanced user capacity through spatial diversity [19]. However, the utilization of a large and dense antenna array brings about strong mutual coupling between different radiator elements [20]. As a result, this leads to a classical issue of antenna scan impedance, which can vary over a substantial range during beam steering [21]. In recent studies, the mismatch of active antenna impedance can be up to 6:1 voltage standing wave ratio (VSWR) during beam scanning [22], [23]. As the direct preceding stage of the antenna, the PAs in the array are subject to a constantly changing load that leads to a performance fluctuation in terms of linearity, stability, output power and efficiency.

To solve the issue of load mismatch for PAs in array systems, there have been multiple types of solutions until now. Conventionally, a circulator/isolator can be placed between the PA and antenna load, which circumvents the PA-antenna interactions, but the typical ferrite-based isolators are expensive, nonintegrable, and bulky preventing the massive scale deployment in the array systems. Alternatively, a tunable matching

network can be inserted between PA and antenna to dynamically compensate for the antenna impedance mismatch [24], [25], [26], [27]. However, all of these solutions require a complex feedback control loop involving sensing and execution units as well as extra tuning components, which significantly complicate the system-level implementation and increase loss, cost, and size. Therefore, it is of great interest to integrate the tuning into the PA stage, and multiple reconfiguration-based load-insensitive PA topologies have been reported recently. In [28], [29], [30], and [31], several quadrature-coupler-based reconfigurable Doherty PA (DPA) are implemented by utilizing exchangeable gate biasing, adaptive power splitting ratio, and tunable carrier-peaking phase offset to configure different DPA operation modes at different load mismatch conditions, so as to compensate for the performance degradation. A similar method is reported in [32] that presents a generic representation of a multiport load-modulation combiner offering tolerance to load mismatch, extended bandwidth, and adjustable OBO range through reconfiguration. Moreover, a series of load-insensitive Doherty PAs are introduced in [33] and [34], which leverages variable dc supply voltage and multiinput phase tuning to maintain the PA performance under a varying load impedance. In summary, it is important to note that the existing solutions mostly require accurate sensing of load impedance as a complex value as well as concurrent reconfiguration of multiple control parameters, leading to high complexity, energy overhead, and latency at the system level.

In this work, based on the horizon of PD-LMBA [7] with control amplifier (CA) as carrier device and balanced amplifier (BA) as peaking, a comprehensive analysis and theoretical derivation for 1-D reconfiguration against load mismatch are presented for the first time in this article. Initially, a generalized theory of mismatch-resilient PD-LMBA is analytically established that comprises different operations of PD-LMBA in low-power region and high-power load-modulation region. It is mathematically unveiled that the quadrature balance of BA is still valid in PD-LMBA, which is based on a unique derivation technique by featuring CA as a duality between the current source (CS) and the voltage source (VS). Taking full advantage of BA's inherent tolerance to load mismatch, the reconfiguration of the entire PD-LMBA is only necessary for the supply voltage of CA with respect to the real part of complex load impedance ideally, as shown in Fig. 1. As such, the control and sensing complexity at the system level is minimized to the lowest level as compared to other reported works, while no tuning elements are needed. The theoretical derivation is effectively verified by circuit simulation using an emulated PD-LMBA model. It is also important to note that the mismatch-resilient operation of PD-LMBA can be easily extended to a broad frequency range given the wideband nature of PD-LMBA. Based on the developed theory, a prototype design of a 1.7–2.9 GHz wideband mismatch-resilient PD-LMBA is experimentally presented, which not only exhibits the desired back-off efficiency enhancement at 50-Ω load but also achieves a first-ever wideband mismatch-resilient operation (i.e., up to 72.8% of efficiency at peak power and 65.4% efficiency down to 10-dB OBO) under 2:1 VSWR. Furthermore, the measurement

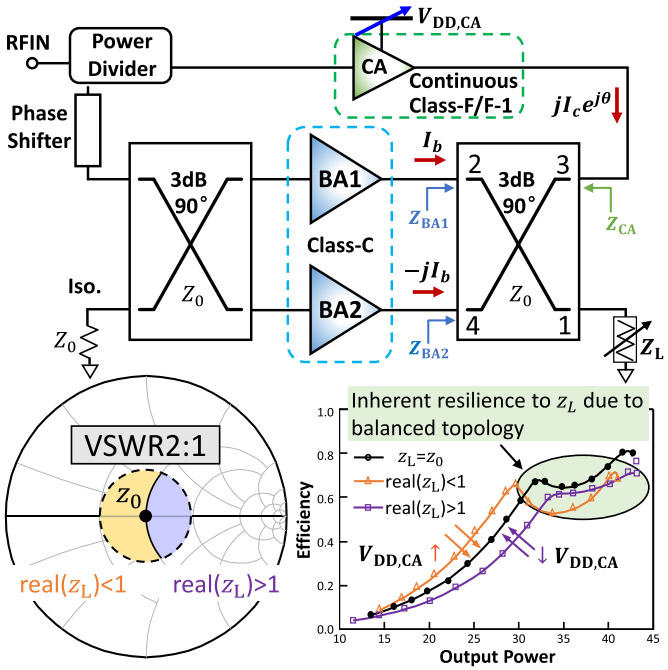

Fig. 1. Overview of mismatch-resilient PD-LMBA with 1-D reconfiguration of $V_{DD,CA}$.

results using continuous-wave and modulated signals clearly outperform state-of-the-art for both nominal matched load and 2:1 VSWR, which solidly demonstrate the effectiveness of the proposed method and hold promising potential for application to array-based massive MIMO systems.

II. Theory of Mismatch-Resilient PD-LMBA

Although the performance of LMBA under load mismatch was preliminarily explored in [35], until now, there have not been any comprehensive theoretical analysis and systematic design methodology. Based on the reported PD-LMBA [7], its mismatch resilience through 1-D reconfiguration is analyzed in this section. As illustrated in Fig. 1, the PD-LMBA consists of a CA (carrier) and balanced amplifier (peaking), it differs from a classic LMBA by biasing the balanced amplifier to Class-C as peaking amplifier and setting CA as carrier amplifier targeting for an extended range (up to 10 dB) of OBO and enhanced back-off efficiency. The load-modulation of PD-LMBA can be modeled as three excitation sources driving the output quadrature coupler. The load-modulation of PD-LMBA can be modeled as three excitation sources driving the output quadrature coupler, and it can be analytically described using the impedance matrix introduced in the following matrix:

$$\begin{bmatrix} V_1 \\ V_2 \\ V_3 \\ V_4 \end{bmatrix} = Z_0 \begin{bmatrix} 0 & 0 & +j & -j\sqrt{2} \\ 0 & 0 & -j\sqrt{2} & +j \\ +j & -j\sqrt{2} & 0 & 0 \\ -j\sqrt{2} & +j & 0 & 0 \end{bmatrix} \begin{bmatrix} I_1 \\ I_2 \\ I_3 \\ I_4 \end{bmatrix} \quad (1)$$

where $V_1 = -I_1/Z_0$, $I_2 = I_{b1}$ and $I_4 = -jI_{b2}$, representing the input RF currents from BA1 and BA2, while $I_3 = jI_c e^{j\theta}$ denotes the CA current. Using the matrix above, the load impedances of BA1, BA2 and CA under matched conditions

can be calculated as

$$Z_{\mathrm{BA1}} = Z_{\mathrm{BA2}} = Z_0\left(1 + \frac{\sqrt{2}I_c e^{j\theta}}{I_b}\right)\Bigg|_{Z_{\mathrm{L}}=Z_0} \tag{2}$$

$$Z_{\mathrm{CA}} = Z_0\Big|_{Z_{\mathrm{L}}=Z_0}. \tag{3}$$

A. Inherent Mismatch Resilience of Balanced PA

The balanced architecture has an inherent mismatch tolerance due to the directivity of the quadrature hybrid coupler. It can be analytically described using the impedance matrix introduced in (1) that, by incorporating isolation at port 3 with a Z_0 termination and load mismatch $Z_{\mathrm{L}} = -V_1/I_1$ at port1, the normalized impedances of BA1 and BA2 with respect to Z_{L} are given by

$$z_{\mathrm{BA1}} = \frac{3z_{\mathrm{L}} - 1}{z_{\mathrm{L}} + 1}, \quad z_{\mathrm{BA2}} = \frac{3 - z_{\mathrm{L}}}{z_{\mathrm{L}} + 1}. \tag{4}$$

Hence, the relationship between z_{BA1} and z_{BA2} in balanced amplifier can be written as

$$z_{\mathrm{BA1}} + z_{\mathrm{BA2}} = 2 \tag{5}$$

$$\text{or} \quad \frac{z_{\mathrm{BA1}} + 1}{z_{\mathrm{BA2}} + 1} = z_{\mathrm{L}}. \tag{6}$$

Equation (5) indicates that the sum of normalized impedances of two sub-amplifiers in the balanced topology are constant and equal to 2. This means that when the balanced amplifier is under load mismatch conditions, the impedance variations of the two identical amplifiers present an opposite trend from the optimum value. Equation (6) is another dependence between z_{BA1} and z_{BA2} that can be derived from (4).

For PD-LMBA, where the isolation-port termination is replaced with a CS, $I_3 = jI_c$, it is found that only (6) is inherited from the balanced amplifier, which can be derived from (1) with the corresponding setting at each port. Clearly, there is a correlation between the conventional quadrature-balanced amplifier and the peaking amplifier (BA) of PD-LMBA, which could potentially be endowed with load insensitivity when it turns on at the predefined OBO.

B. 1-D Reconfiguration of PD-LMBA for Mismatch Compensation in Low-Power Region ($P_{\mathrm{OUT}} < P_{\mathrm{Max}}/\mathrm{OBO}$)

In the low-power region with CA solely operating, this analysis can be considered as a single PA circuit under the load-mismatch condition, where the quadrature coupler with BA1 and BA2 ports open-circuited acts as an inverter shown in Fig. 2(a). The transistor as a CS is approximated by a piecewise linear model [36]. Its normalized load impedance z_{CA} ($= Z_{\mathrm{CA}}/Z_0$) is directly inverted from z_{L} by the quadrature coupler, and the normalized representation is given by

$$z_{\mathrm{CA,LP}} = 1/z_{\mathrm{L}} = y_{\mathrm{L}}. \tag{7}$$

To theoretically analyze the CA under mismatch, the first step is to calculate the output power of the CA [33]. It is calculated from a fundamental voltage component of CA (V_c) and load (Z_{CA}) as the following expression:

$$P_{\mathrm{CA}} = \frac{1}{2}\mathrm{real}(Z_{\mathrm{CA}})\left(\frac{|V_c|}{|Z_{\mathrm{CA}}|}\right)^2. \tag{8}$$

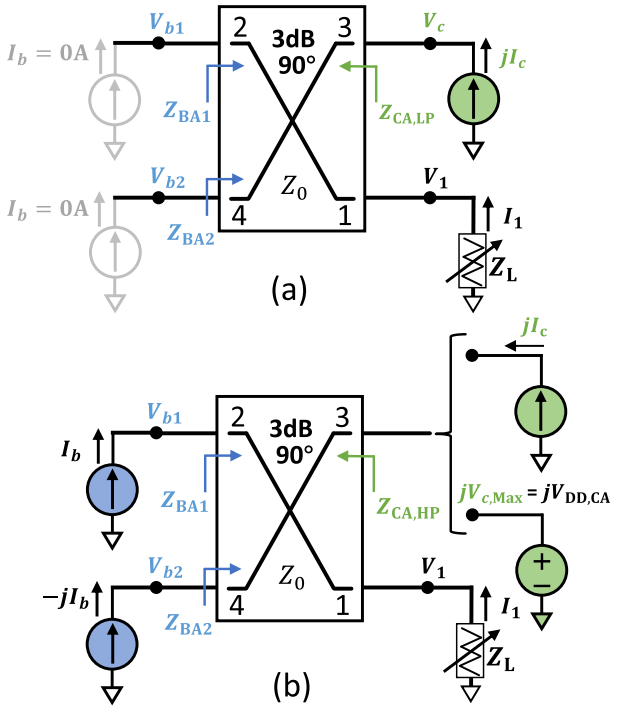

Fig. 2. Ideal generalized schematic of the output combining network for analyzing the proposed PD-LMBA architecture: (a) low-power region where $P_{\mathrm{OUT}} < P_{\mathrm{Max}}/\mathrm{OBO}$, (b) high-power region where $P_{\mathrm{Max}}/\mathrm{OBO} \leq P_{\mathrm{OUT}} \leq P_{\mathrm{Max}}$. (The CA is expected to remain saturated in this region which can feature a unique CS-VS duality.)

The corresponding saturation power of CA at the matched load with the highest efficiency can be written as

$$P_{\mathrm{CA,Sat.0}} = \frac{V_{\mathrm{DD,CA0}}^2}{2Z_0}\Bigg|_{Z_{\mathrm{L}}=Z_0}. \tag{9}$$

where Z_0 is the nominal matched load, and $V_{\mathrm{DD,CA0}}$ is the corresponding nominal dc bias voltage. For PD-LMBA, it is critical to set $P_{\mathrm{CA,Sat.0}} = P_{\mathrm{OBO}}$ that ensures the first efficiency peak.

For an arbitrary load impedance, the CA saturation power can be re-derived as

$$P_{\mathrm{CA,Sat.}} = \frac{V_{\mathrm{DD,CA}}^2}{2Z_0}\frac{\mathrm{real}(z_{\mathrm{CA}})}{|z_{\mathrm{CA}}|^2}. \tag{10}$$

In order to keep $P_{\mathrm{CA,Sat.}}$ constantly equal to its nominal value at the matched load (for maintaining a constant first efficiency peak at the designated P_{OBO} as depicted in Fig. 1, it is necessary to enforce the following condition:

$$P_{\mathrm{CA,Sat.}}\left(V_{\mathrm{DD,CA}}\right) = P_{\mathrm{CA,Sat.0}} \tag{11}$$

which is achieved by reconfiguring the CA dc bias voltage, $V_{\mathrm{DD,CA}}$. By solving (11), $V_{\mathrm{DD,CA}}$ should be dependent on z_{CA}

$$V_{\mathrm{DD,CA}} = V_{\mathrm{DD,CA0}}\frac{|z_{\mathrm{CA}}|}{\sqrt{\mathrm{real}(z_{\mathrm{CA}})}}. \tag{12}$$

By replacing z_{CA} with $1/z_{\mathrm{L}}$ as expressed in (7), the above expression can be rewritten as

$$V_{\mathrm{DD,CA}} = V_{\mathrm{DD,CA0}}\sqrt{\frac{1}{\mathrm{real}(z_{\mathrm{L}})}}. \tag{13}$$

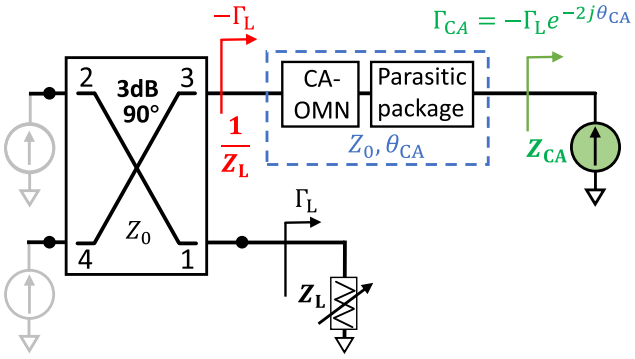

Fig. 3. Phase shift of CA output network and Γ in different planes.

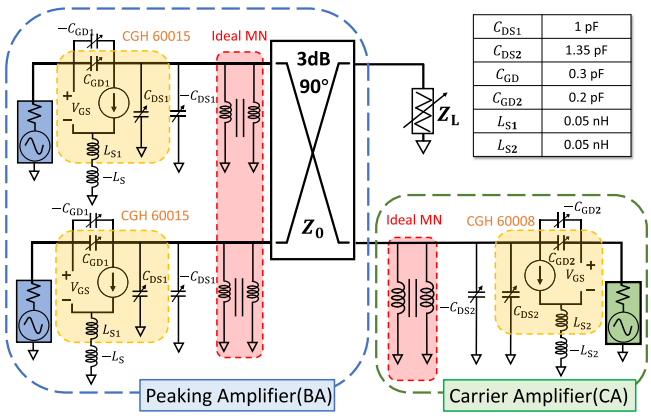

Fig. 4. Emulated model setup of the proposed PD-LMBA with bare-die GaN transistors for verification.

It is interesting to note that the reconfigurable dc bias voltage of CA is only related to the real part of load impedance, z_L. For high-resistance loads (i.e., real(z_L) > 1), $V_{DD,CA}$ should be lower than the nominal value ($V_{DD,CA0}$) in order to maintain a constant saturation power of CA. Vice versa, $V_{DD,CA}$ should be increased from $V_{DD,CA0}$ for low-resistance loads (i.e., real(z_L) < 1).

It is important to note that the most commonly used sensing method of the load is based on a directional coupler, where the reflection coefficient Γ_L is easier to obtain rather than the load impedance z_L. Also, in a practical PD-LMBA design, the CA contains an output matching network (OMN). Unlike the theoretical model in Fig. 2, the current-generation plane of the realistic CA is not directly connected to the coupler isolation port but through the parasitic network and CA OMN. Thus, the control of $V_{DD,CA}$ is re-derived based on Γ_L with the realistic model shown in Fig. 3. The overall phase shift caused by parasitic network and CA OMN can be represented as a transmission line of phase θ_{CA}, and the corresponding Γ at different planes are illustrated in Fig. 3. The Γ_L-dependent $V_{DD,CA}$ can be derived based on as follows:

$$V_{DD,CA} = V_{DD,CA0}\sqrt{\frac{1+|\Gamma_{CA}|^2+2\text{real}(\Gamma_{CA})}{1-|\Gamma_{CA}|^2}} \tag{14}$$

$$= V_{DD,CA0}\sqrt{\frac{1+|\Gamma_L|^2-2\text{real}\left(\Gamma_L e^{-j2\theta_{CA}}\right)}{1-|\Gamma_L|^2}}\Bigg|_{|\Gamma_{CA}|=|\Gamma_L|}. \tag{15}$$

In order to maximize the first efficiency peak at the target power back-off, CA is designed with continuous Class-F mode which can deliver over 80% ideally [37]. Combined with the reconfiguration of $V_{DD,CA}$, the saturation power of CA can be well maintained at 10-dB OBO with a consistent first efficiency peak against arbitrary load mismatch, which can ensure the highest possible efficiency across the entire OBO range.

C. Intrinsic Mismatch Resilience of PD-LMBA in High-Power Load-Modulation Region ($P_{OUT} > P_{Max}$/OBO)

When CA is driven to its saturation at P_{OBO}, an ideal phase offset between BA and CA (assuming $\theta = 0$) is implemented, and CA can be considered as either a CS due to the intrinsic nature of the transistor or a constant VS due to the fact that it should remain saturation during load modulation. At the same P_{OBO}, the BA turns on and is load-modulated by the CA. The load impedance of CA is given by

$$z_{CA,HP} = \frac{1}{z_L} + \sqrt{2}\frac{I_b}{I_c}\left(\frac{1}{z_L} - 1\right). \tag{16}$$

Although the CA impedance is modulated as a function of I_c under load mismatch, the increase of input power due to the Wilkinson divider constantly drives CA into saturation that most likely can be sustained throughout the load-modulation region. Given this constant saturation, CA features a duality between CS and VS, as shown in Fig. 2(b). When considering CA as a CS, I_c the normalized impedance of BA1 and BA2 under load mismatch can be calculated as

$$z_{BA1} = \frac{\sqrt{2}I_c}{I_b} + 1 \tag{17}$$

$$z_{BA2} = \left(2 + \frac{\sqrt{2}I_c}{I_b}\right)\frac{1}{z_L} - 1. \tag{18}$$

From a different perspective that CA ideally remains voltage saturated in this region, it thereby can be considered as a VS, and the BA impedances are re-derived as

$$z_{BA1} = \left(2 + \frac{\sqrt{2}V_c}{Z_0 I_b}\right)z_L - 1 \tag{19}$$

$$z_{BA2} = 1 + \frac{\sqrt{2}V_c}{Z_0 I_b}. \tag{20}$$

Equations (18) and (19) unveil an important fact that the impedances of BA1 and BA2 have z_L and $1/z_L$ dependence, respectively, so that their operations can complement each other under load mismatch similar to the generic balanced amplifier. Meanwhile, it is important to note that although (17) and (20) are mathematically valid, they are not physically meaningful since neither BA1 nor BA2 should be Z_L-independent. Just like the Wave-Particle duality of light, the CA in PD-LMBA presents a VS-CS duality: CA is a VS (VS) to BA1 and a CS (CS) to BA2.

Overall, as long as the 1-D reconfiguration of CA (i.e., load-dependent $V_{DD,CA}$) maintains a constant $P_{CA,Sat.} = P_{OBO}$,

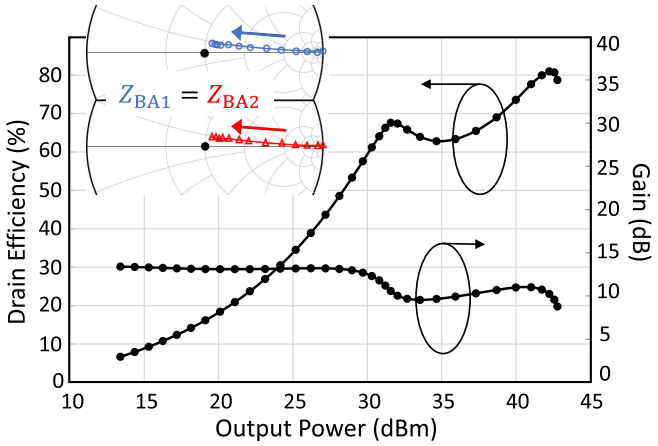

Fig. 5. Simulated efficiency and gain versus P_{OUT} of emulated PD-LMBA model and load-modulation trajectory of BA1 and BA2 under matched load.

the inherent "balance" between BA1 and BA2 makes the entire PD-LMBA mismatch resilient that is sustained from low-power region to load-modulation region.

III. Verification Using Emulated PD-LMBA Model

To verify the mismatch-resilient PD-LMBA theory proposed in Section II, an ideal PD-LMBA model is emulated using two different types of bare-die GaN transistors, ideal quadrature couplers, and ideal transformers for impedance matching, as shown in Fig. 4. Specifically, BA1 and BA2 are built with CGH60015 model from Wolfspeed, and CA is built with a smaller-sized model CGH60008 due to its lower output power than BA. Using the dedicated designed negative capacitance ($-C_{DS}$, $-C_{GD}$) and negative source-degeneration inductance ($-L_S$), the intrinsic parasitics of transistors are fully de-embedded. Therefore, the emulate models can well imitate ideal transistor devices as voltage-controlled CSs. The established emulation model of the entire PD-LMBA is simulated in ADS. The simulation results are plotted in Fig. 5 including efficiency and gain profiles as well as the load-modulation trajectories of BA1 and BA2 (identical at $Z_L = Z_0$).

A. Emulated Balanced Amplifier Under Mismatch

To first verify the theory in Section II-A, a balanced PA is built by using the emulation model with a termination impedance ($Z = 50\ \Omega$) at the isolation port. The resilience of the balanced amplifier circuit to load mismatch on the 2:1 VSWR circle is simulated. Fig. 6 shows the impedances of BA1 and BA2 under different load conditions. The simulation results clearly indicate that the impedances of BA1 and BA2 always present opposing deviations from the optimum value, and their sum of normalized impedances are constantly equal to 2 as expected from the theoretical relationship in (5). The simulation results agree well with the mathematical derivation and results in Section II-A, which solidly proves the theory of quadrature-balanced amplifier with complementary behaviors of BA1 and BA2 under load mismatch.

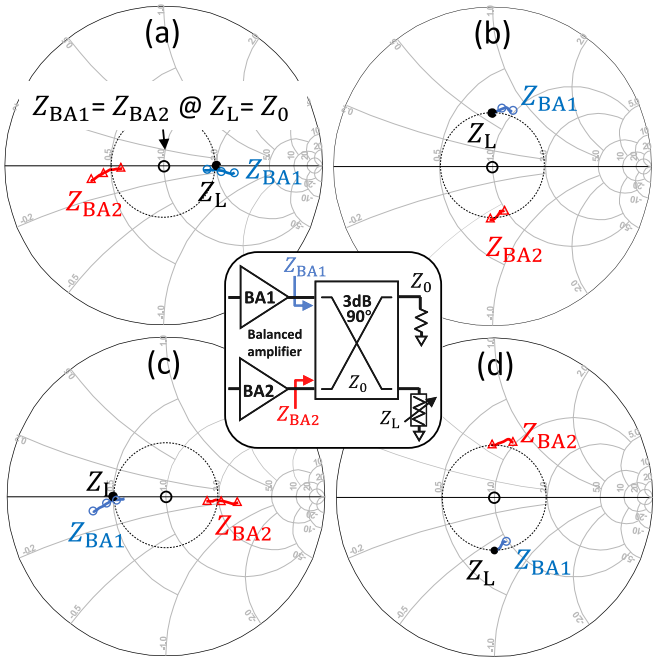

Fig. 6. Load mismatch analysis of Balanced Amplifier for representative cases on VSWR 2: 1 circle: (a) $|\Gamma_L|\angle 0°$, (b) $|\Gamma_L|\angle 90°$, (c) $|\Gamma_L|\angle 180°$, and (d) $|\Gamma_L|\angle 270°$.

B. Emulated PD-LMBA Model: Mismatch Resilience in Low-Power Region Through 1-D Reconfiguration

The analytical derivations described in Section II-B demonstrates the theory of utilizing 1-D tuning the supply voltage of CA (carrier) with respect to the real part of load impedance, which maintains a constant saturation power of CA at the pre-defined OBO. The theory is validated by simulation using the developed emulation model in this section. According to Fig. 7(a)–(c), the impedance of CA (z_{CA}) is directly inverted from z_L, which proves (7). Fig. 7(d) shows that the corresponding supply voltage (V_{CA}) of control amplifier is solely dependent on the real part of load impedance (z_L), and the CA saturation power can be maintained at nearly the same OBO (roughly 10 dB from the peak) against different mismatch conditions, thus ensuring the desired CS-VS duality of CA for the subsequent operation of the peaking amplifier (BA). In a word, the simulation results matches the derivations in Section II-B, and therefore, the theory is firmly proven.

C. Emulated PD-LMBA Model: Intrinsic Mismatch Resilience in High-Power Load-Modulation Region

When CA reaches to its saturation, BA1 and BA2 turns on simultaneously, and the load modulation starts. The impedances of BA1 and BA2 are close to open-circuit at the beginning of load modulation as shown in Fig. 5 (inset Smith chart). Fig. 8 shows the simulated fundamental current and voltage of BA1, BA2, and CA, respectively, while Fig. 9 depicts the load modulation trajectories of three PAs under mismatch. Four representative load values on the 2:1 VSWR circle are selected to specifically elaborate the load modulation behaviors of BA1, BA2 and CA under different mismatch conditions.

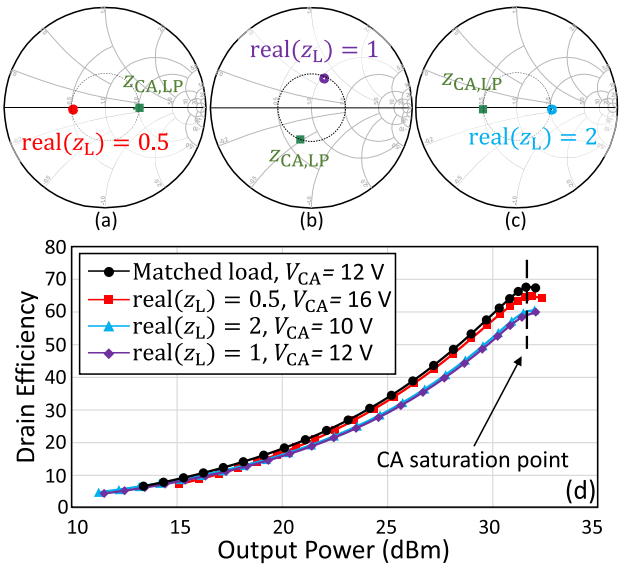

Fig. 7. 1-D reconfiguration of CA for mismatch-resilient operation at low-power region, i.e., $P_{CA,Sat.} = P_{OBO}$ against VSWR: (a)–(c) impedance trajectory of CA at low power region ($z_{CA,LP}$) inverted from real part of different load impedance z_L; (d) simulated DE versus output power with corresponding $V_{DD,CA}$ at different load condition.

1) *High-Resistance Load ($z_L = 2$)*: In this condition, when CA saturates, the BA currents, I_{b1} and I_{b2}, start to increase while the V_c maintains almost the same level, as shown in Fig. 8(a). In this case, the CA behavior indicates a clear CS-VS duality, and thus, the load impedances of BA1 and BA2 are properly modulated with a complementary dependence of z_L according to (17) and (18), i.e., $Z_{BA1} \propto z_L$ and $Z_{BA2} \propto 1/z_L$. Moreover, the CA load impedance becomes higher with an increasing I_b according to (16) in which $(1/z_L - 1) < 0$, shown in Fig. 9(a). Nevertheless, the drop of CA power during load modulation only results in a trivial impact on the overall PD-LMBA as the output power is mostly generated by BA at this power level. The theoretical derivation is consistent with the simulation results.
2) *Low-Resistance Load ($z_L = 0.5$)*: As indicated by (16), the CA is load modulated like the carrier amplifier in Doherty PA (i.e., $Z_{CA,HP} \propto 1/I_c$) when $|z_L| < 1$. As a result, the CA current surges in the load-modulation region, as shown in Fig. 8(b). This also leads to a sharp increase of Z_{BA2} according to (18) and the clamping of BA2 current, i.e., I_{b2} in Fig. 8(b). The load modulation trajectory of BA2 turns toward open circuit point as demonstrated in Fig. 9(b). Nevertheless, the 'turn-off' of BA2 power is compensated for by the sharp increase in CA power. Together with the unaffected load modulation of BA1 and I_{b1} as depicted in Fig. 8(b) and Fig. 9(b), respectively, the overall peak output power of PD-LMBA should remain unchanged. (*Note*: Although the load modulation of CA breaks its CS-VS duality at z_L=0.5, it makes CA substitute the role of BA2 so as to re-establish the balance with BA1.)

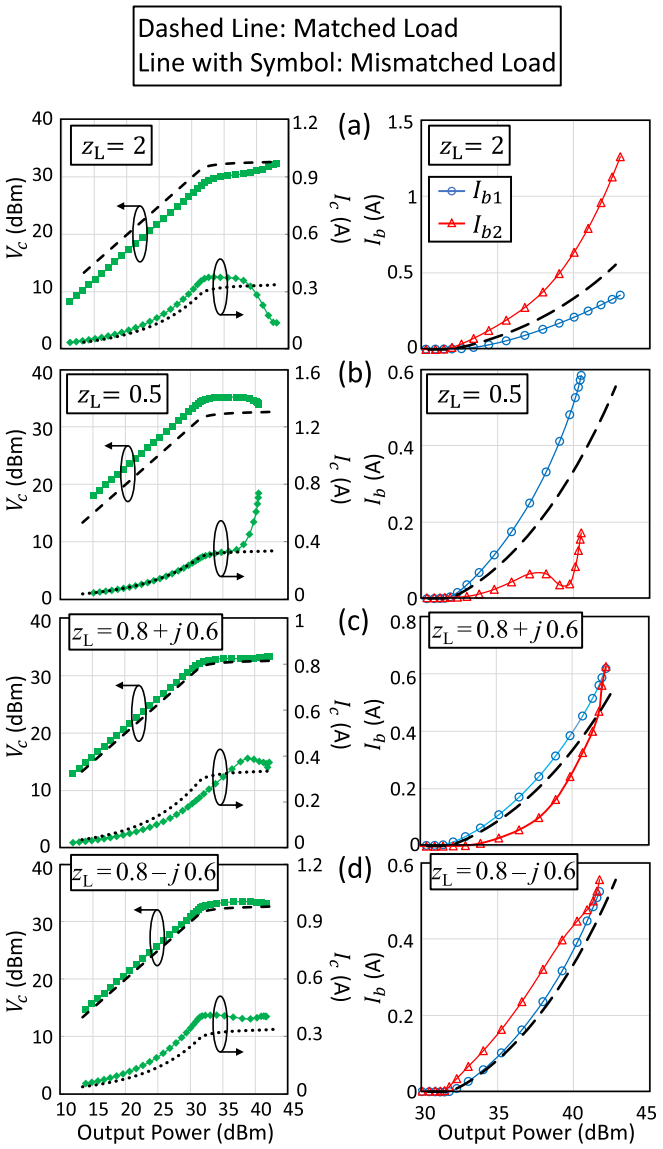

Fig. 8. Simulated BA1, BA2, and CA currents and voltages using emulated PD-LMBA model at 1.7 GHz for different loads on VSWR 2:1 circle. (a) $z_L = 2$. (b) $z_L = 0.5$. (c) $z_L = 0.8 + j0.6$. (d) $z_L = 0.8 - j0.6$.

3) *Complex Loads:* For the normalized load impedance corresponding to the two reactive points $z_L = 0.8 + j0.6$ and $z_L = 0.8 - j0.6$, the CA well maintains a constant VS and nearly constant CS, thus offering the desired "balance" between BA1 and BA2 as shown in Fig. 9 where $Z_{L,BA1}$ and $Z_{L,BA2}$ are conjugate during load modulation. As a result, the BA currents are almost identical and equal to that in the matched condition, leading to a consistent output power and efficiency of the overall PD-LMBA.

Fig. 10 shows the overall efficiency and gain profiles of different load conditions. With the tuning of CA supply voltage, V_{CA}, the first efficiency peak can be kept constantly around 10-dB OBO. In the high-power load-modulation region, the overall performance can be maintained due to the inherent mismatch resilience of the balanced amplifier. It is demonstrated that the efficiency profile at matched load can be well

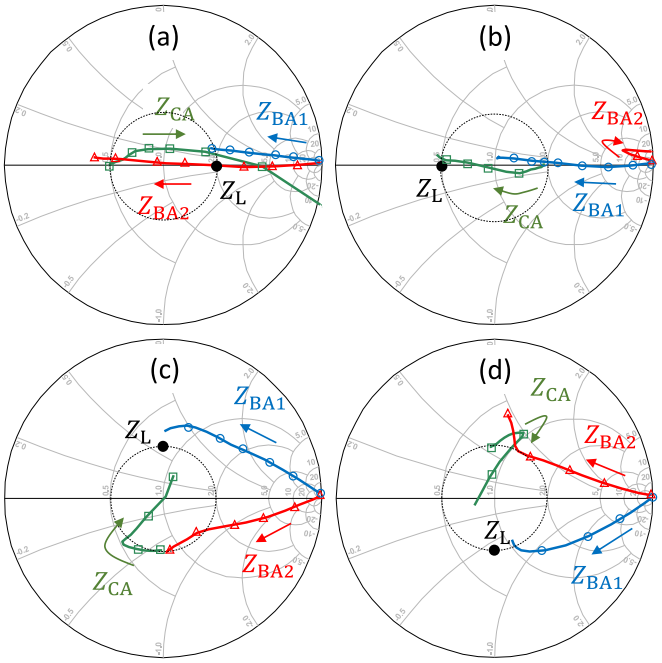

Fig. 9. Load modulation analysis of PD-LMBA for representative cases on VSWR 2: 1 circle. (a) $|\Gamma_L|\angle 0°$. (b) $|\Gamma_L|\angle 180°$. (c) $|\Gamma_L|\angle 90°$. (d) $|\Gamma_L|\angle 270°$.

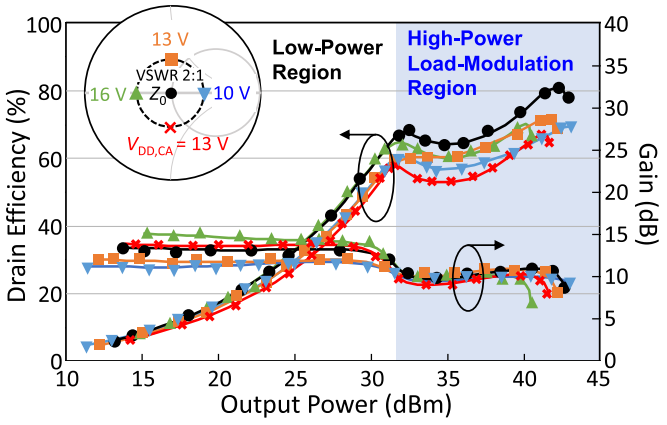

Fig. 10. Simulated efficiency and gain versus P_{OUT} of emulated PD-LMBA model under different load conditions shown in Smith chart.

maintained against 2:1 VSWR with the 1-D reconfiguration. Therefore, the theory presented in Section II is solidly proven.

IV. Practical Design of Wideband PD-LMBA With Continuous-Mode Matching

To verify the proposed theory, an RF-input PD-LMBA is designed with a target frequency range from 1.7 to 2.9 GHz. The practical design of the prototype is similar to the authors' other work on hybrid asymmetrical LMBA presented in [37], while the circuit is re-optimized for PD-LMBA operation. Specifically, two 10-W GaN HEMTs (CG2H40010F) from Wolfspeed are used for both CA and BA. In order to accommodate the high PAPR of emerging 5G signals, a back-off range of 10 dB is selected for this prototype.

The BA input coupler is built with a commercial component (IPP-7118, available from Innovative Power Products) widely operating at 1.7–2.9 GHz. The output coupler of BA is

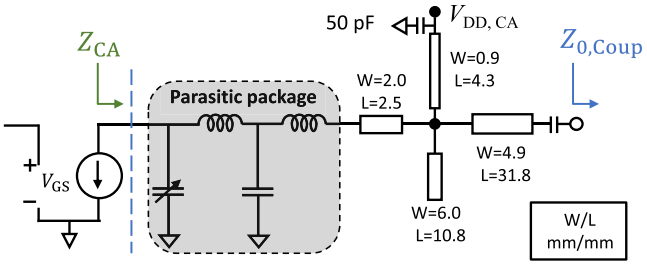

Fig. 11. Schematic of the designed CA OMN.

implemented with a non-50-Ω three-stage branch-line hybrid structure [38], which can provide sufficient bandwidth and also serve as a part of an output impedance matching network (OMN). The OMN of BA is realized by the cooperation of impedance transformer coupler and bias lines. This leads to the reduction of the broadband phase dispersion that normally occurs in the complex matching network [8], so as to realize the equalization of the phase changes of BA and CA in the broadband range. The detailed design of BA and CA as well as the wideband phase BA-CA alignment is illustrated in Sections IV-A–IV-C.

A. Wideband CA Design in Continuous Mode

At the low output power level with only the CA operating, the two ports of BA1 and BA2 are close to an open circuit and can be equivalent to R-C tanks [37]. To fulfill this low output power, CA is executed with the 10-W GaN transistor (Wolfspeed CG2H40010), and it is biased in Class-AB mode with a reduced supply voltage, i.e., around 10 V of $V_{DD,CA}$. In order to cover the entire target-wide bandwidth with the enhanced back-off efficiency, the output matching network (OMN) of CA requires a complex harmonic-tuned structure that normally engenders an unexpected phase dispersion [8]. This could be contradictory to the phase control requirement of BA, especially for wideband design. Thus, a simplified TL-based OMN instead of multistage ladder network [39] is selected to meet the requirement of the wideband CA design with the highest-possible first efficiency peak and meanwhile ease the wideband phase control of PD-LMBA.

Fig. 11 shows the designed TL-based OMN of CA [37], similar to [37]. This structure can reduce the phase dispersion since it only includes one shunt stage with a bias line and open stub. The phase offset line at the input of BA can perfectly counteract the phase shift of the series components of CA OMN. On the other hand, based on [37], the harmonic-tuned OMN can convert the nominal impedance of isolation port to the harmonic impedance of continuous Class-F (CCF) and continuous Class-F^{-1} (CCF^{-1}) modes, which enhance the maximum first efficiency peak across the band.

B. Wideband BA Design

In order to build a balanced amplifier, the two peaking devices are implemented by two identical 10-W packaged GaN transistors (CG2H40010) and designed under the same gate bias voltage with an identical matching method as shown in

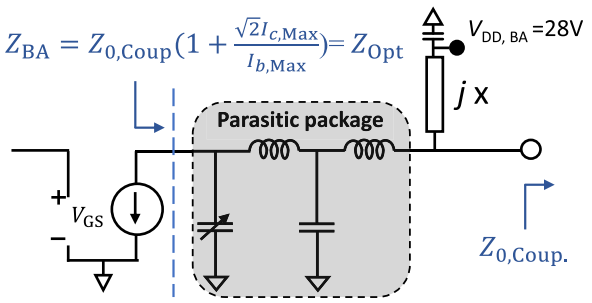

Fig. 12. Schematic of the designed BA OMN.

Fig. 12. The input wideband quadrature (1.7–2.9 GHz) coupler is built using a commercial product (IPP-7118) and the output coupler is implemented with a non-50-Ω three-stage branch-line coupler [38] which well satisfies the design requirement of bandwidth.

To simplify the load-modulation control of BA and reduce the phase dispersion effect, a similar design method of OMN to that is presented in [40] and [41] is utilized as shown in Fig. 12. In this design, the OMN of BA is simplified as a shunt inductance (jX) implemented by a bias line, which effectively cancels the parasitic network that is dominated by C_{DS} of the transistor. Based on the derivation of Z_{BA} in (2), when two BAs reach the maximum power under load modulation ($I_b = I_{b,Max}$), the load impedance presented to the intrinsic drain of BA is equal to $Z_{0,Coup}$ multiplied by a load-modulation factor, given an ideal phase offset, i.e., $\theta = 0$, as the equation indicated in Fig. 12. By properly setting the value of $Z_{0,Coup}$, the impedance of two BA, Z_{BA}, at peak power can be equal to Z_{OPT}. Since BA is biased in Class-C mode, we found in the simulation that the harmonic tuning is not as critical as it is for CA.

Following the well-known input matching method as presented in [38], a four-stage low-pass TL input matching network is implemented covering the target bandwidth from 1.7 to 2.9 GHz. Each stage includes a series L (high impedance TL) and a shunt C (low impedance open stub). This entire network is synthesized by the CAD-based optimizer to offer an optimal wideband matching.

C. Wideband BA-CA Phase Offset Analysis and Design

To qualitatively analyze the phase difference between the BA and CA, the signal paths o f BA and CA are illustrated in Fig. 13(a) and (b). The BA signal starting from the input port of the first quadrature coupler is divided into I (in-phase signal) and Q (quadrature signal) which then travel through BA1 and BA2, respectively, and are finally combined at the output port of the second quadrature coupler as shown in Fig. 13(a). Overall, the BA path delay involves I and Q paths of input and output quadrature couplers, respectively, and the amplifier stage including an input matching network (IMN), OMN and GaN device.

From the perspective of the CA signal, it starts at the input port of CA IMN and passes the GaN device and the OMN of CA. Then, the CA signal is fed into the output coupler of

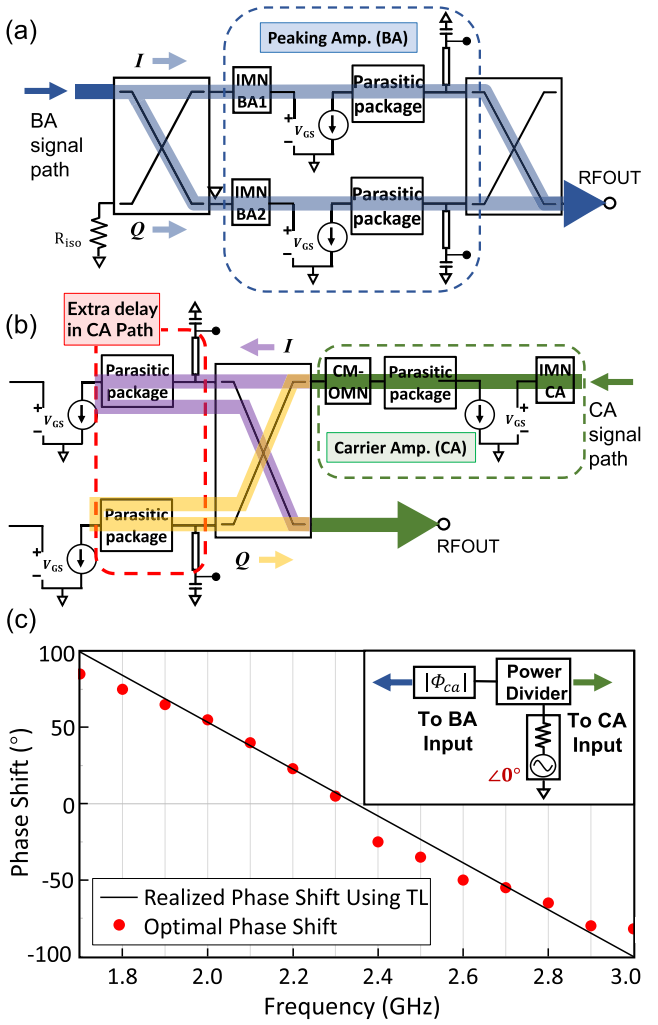

Fig. 13. (a) Signal path of BA; (b) signal path of CA; (c) simulated optimal BA1-CA phase offset at different frequencies and TL-based wideband phase shifter.

BA, where it is also split into I and Q. The I signal travels through the OMN and parasitic network of BA1, which is immediately reflected back when it reaches the intrinsic drain of BA1. This reflected I signal then travels backward through the BA output network and is directed to the output port by the directional coupler. Due to the symmetry of BA, the Q path is identical to the I path as depicted in Fig. 13(b). It is critical to point out that compared to the BA path, the delay of the CA path involves two extra portions, i.e., twice of the BA output network, in which the signal travels back and forth. As the BA output network (the extra delay in the CA path) is designed with the simplest structure of a bias line, this shunt inductor can well resonate with the parasitic network that mainly contains a large C_{DS}, the delay of this network is minimized, and it can be easily compensated for using a delay line at the input of BA.

The above qualitative analysis indicates that if the time delays of CA and BA paths are equalized, a wideband phase alignment is automatically achieved for the optimal PD-LMBA operation. Using the method in [37], it is demonstrated that the optimal phase shift between CA and BA is approximately

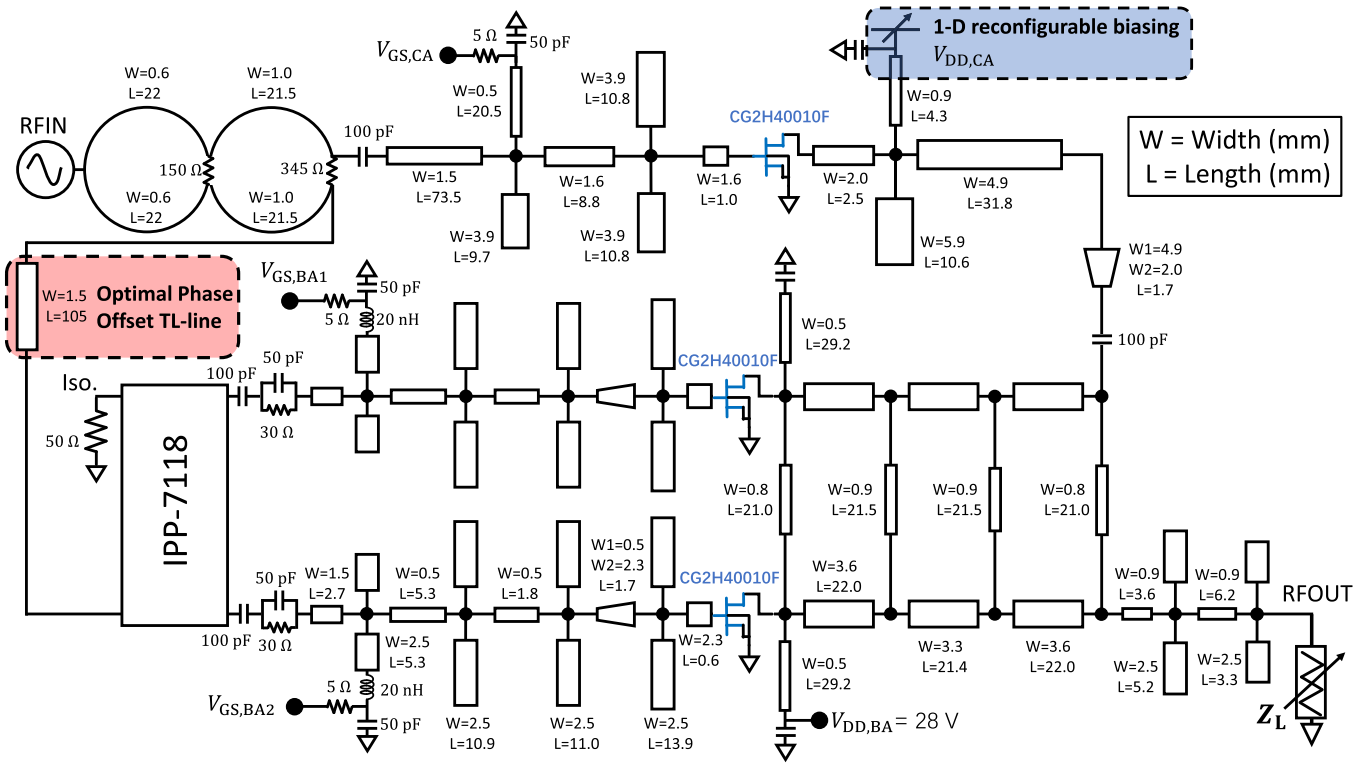

Fig. 14. Circuit schematic overview of designed PD-LMBA.

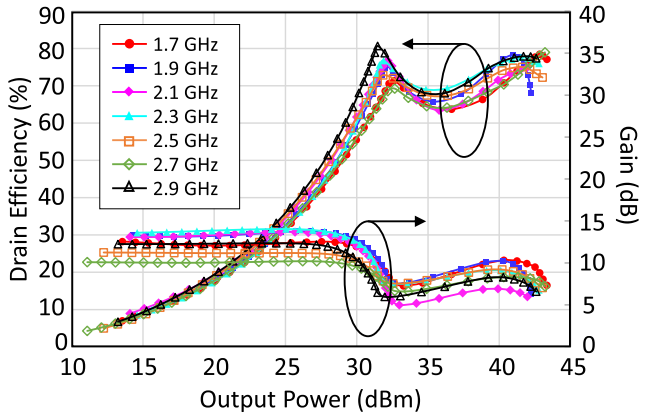

Fig. 15. Simulated drain efficiency and gain under match condition with from 1.7 to 2.9 GHz.

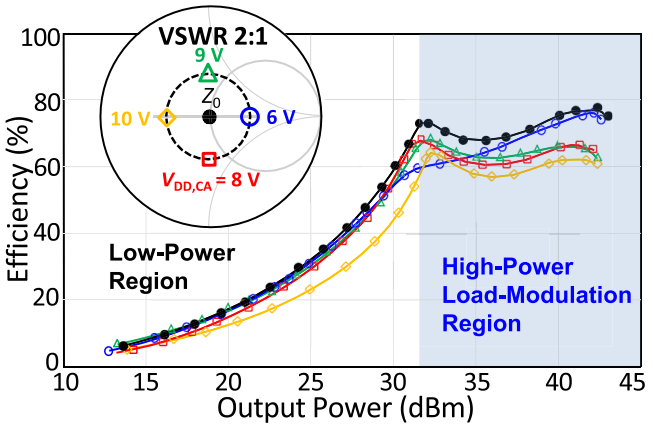

Fig. 16. Simulated efficiency versus P_{OUT} at 2.5 GHz under different load conditions (inset Smith Chart).

linear to frequency proportionally as shown in Fig. 13(c). As a result, the equalization of phase (delay) between BA and CA can be simply resolved by using a 50-Ω transmission line at the input port of BA to fit the wideband phase-offset requirement [7], [40], and [41].

D. Overall Schematic and Simulation Results

The overall designed circuit schematic and the detailed values of all actual circuit elements are shown in Fig. 14. With the detailed design described in this section, the overall efficiency and gain under match conditions are swept with power as shown in Fig. 15. Fig. 16 shows the simulated efficiency at different mismatched load conditions. To make a comparison with the theory and emulated model, the load variation of this practical PD-LMBA design is de-embedded to the coupler plane. It is also found in simulation that the overall phase delay of the CA output network (matching and parasitics), θ_{CA}, is roughly 180°, so that the dependence of $V_{DD,CA}$ and z_L well match the ideal case. These results clearly indicate that the performance of designed PD-LMBA in terms of efficiency profile and maximum output power can be well sustained against 2:1 VSWR with the 1-D reconfiguration of $V_{DD,CA}$.

V. Fabrication and Measurement Results

Fig. 17 shows the measurement system setup and the photograph of fabricated PD-LMBA. The circuit is implemented

TABLE I
COMPARISON WITH STATE-OF-THE-ART OF WIDEBAND LOAD-MODULATED PAS

Ref./ Year	Architecture	Freq (GHz)	P_{Max} (dBm)	DE_{Max} (%)	DE@10dB OBO(%)
[7] 2020	PD-LMBA	1.5 — 2.7	43	58—72	47—58
[13] 2017	LMBA	0.7 — 0.85	42	57—70	30—35* †
[14] 2017	LMBA	1.8 — 3.8	44	46—70	20—25* †
[15] 2018	Dual-Input LMBA	1.7 — 2.5	48—48.9	48—58*	33—45* †
[16] 2020	CM-LMBA	1.45 — 2.45	45.6 — 46.7	67.1—77.9	37—43
[17] 2021	ALMBA	0.55 — 2.2	41—43	49—82	39—64
[18] 2021	H-ALMBA	0.55 — 2.2	42	55—82	40—61
This Work	PD-LMBA	1.7 — 2.9	39.4—43.1	65.3—76.9	54.5—70.5

* Graphically estimated, † PAE

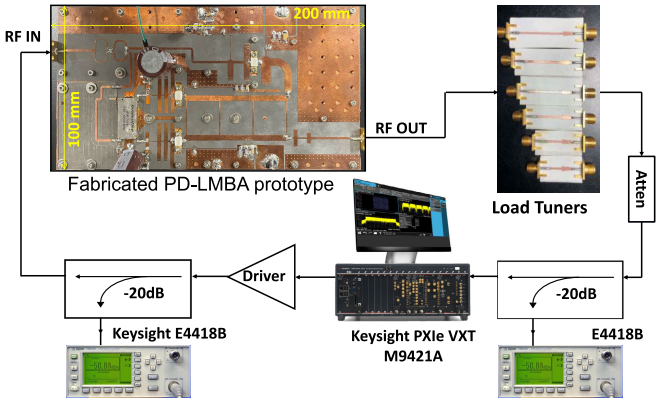

Fig. 17. Fabricated PD-LMBA prototype and testing setup.

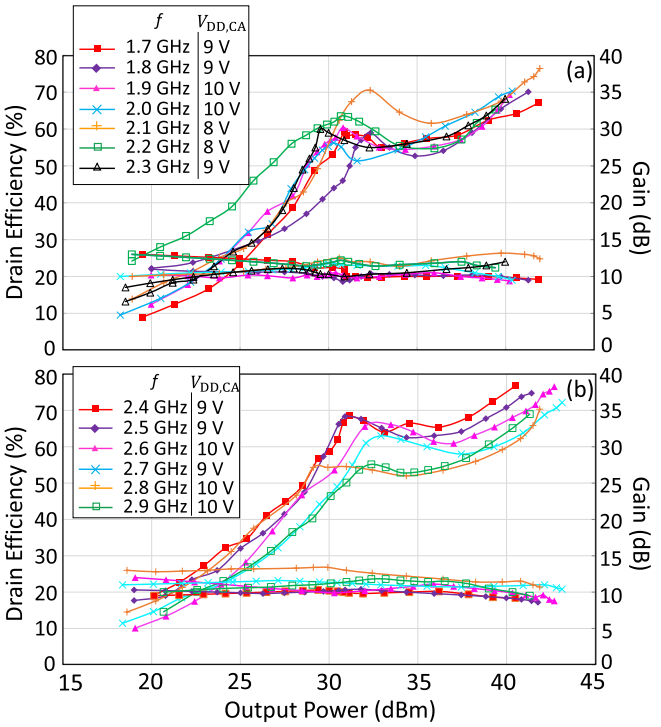

Fig. 18. Measured DE and Gain with CW signal under match condition at (a) 1.7 to 2.3 GHz. (b) 2.4 to 2.9 GHz.

on a 0.5-mm (20-mil) thick Rogers Duroid-5880 PCB board with a dielectric constant of 2.2 and the board size is 200 mm × 100 mm. A Keysight PXIe vector transceiver (VXT M9421) is used as a signal generator and analyzer for CW and modulated measurement. A driver stage provides a power level and a directional coupler after the isolator is used to accurately sample and measure the input power. The PA output is connected to several designed impedance transformer, which covers the 2:1 VSWR circle on Smith Chart with the phase swept at 30° step. The BA is biased in Class-C mode with $V_{GS,BA}$ of −2.8 V. The drain voltage biasing of BA, $V_{DD,BA}$, is set to 28 V to achieve its maximum output power. The CA is biased in Class-F/F^{-1} mode with a $V_{GS,CA}$ of −5 V. $V_{DD,CA}$ is set in an adjustable range from 5 to 12 V to ensure its saturation is maintained at 10-dB power back-off when the load impedance is mismatched.

A. Continuous-Wave Measurement

The fabricated prototype is first measured with a single-tone continuous-wave (CW) stimulus signal from 1.7 to 2.9 GHz at different power levels. Under the condition of a standard matched load impedance of 50 Ω, $V_{DD,CA}$ is around 10V with a minor change to maintain the 10-dB OBO level. The measured efficiency and gain versus output power are plotted in Fig. 18. The proposed PD-LMBA achieves a efficiency of 65.3%–76.9% at peak power and 54.5%–70.5% at 10-dB OBO from 1.7–2.9 GHz. The measured gain is maintained around 8–13 dB at different OBO levels with the saturated output power of 39.4–43.1 dBm across the entire bandwidth. The measured PAE over the entire bandwidth is shown in Fig. 19, showing a clear efficiency enhancement at the power back-off. And the performance of the prototype PA under match condition is summarized and compared with other published works in Tables I and II.

In order to verify the mismatch recovery capability of PD-LMBA through 1-D $V_{DD,CA}$ reconfiguration, three

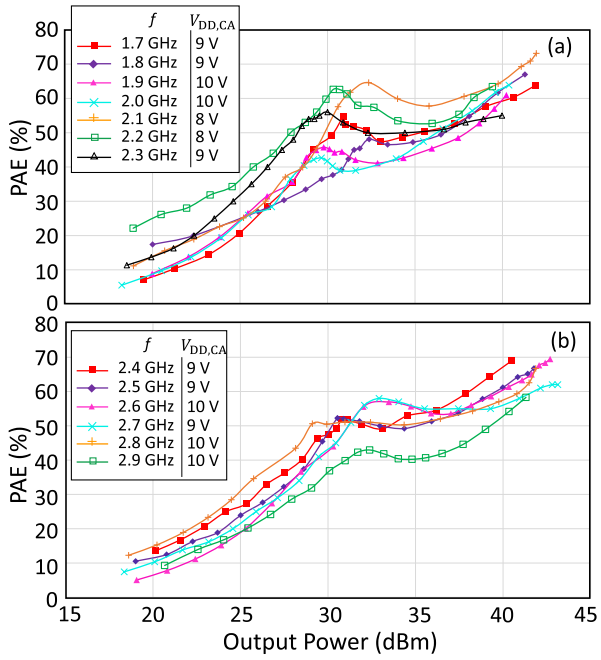

Fig. 19. Measured PAE with CW signal under match condition at (a) 1.7 to 2.3 GHz. (b) 2.4 to 2.9 GHz.

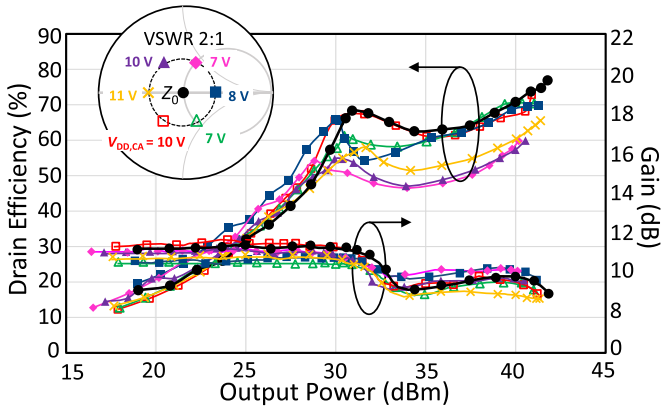

Fig. 20. Measured drain efficiency and gain versus P_{OUT} at 2.5 GHz for different load condition with corresponding reconfigured $V_{DD,CA}$ on VSWR 2: 1 circle shown in inset Smith chart.

representative frequencies, 1.7, 2.1, and 2.5 GHz, are selected for CW measurement with various mismatched loads. As shown in Fig. 17, a set of load tuners are fabricated as a customized load—pull system. At 2.5 GHz, the measured DE and gain versus swept output power at various loads across the 2:1 VSWR circle are shown in Fig. 20. A DE up to 72.8% is measured at a peak power of 41.4 dB under various load mismatch conditions, and the measured DE at 10-dB OBO is up to 65.4%. It is clearly seen that the efficiency profiles under load mismatch well replicate the shape at matched conditions. The measurement is then extended to 1.7 and 2.1 GHz, where DE at peak power and 10-dB OBO are measured versus different phase points on the entire VSWR 2:1 circle, as shown in Fig. 21.

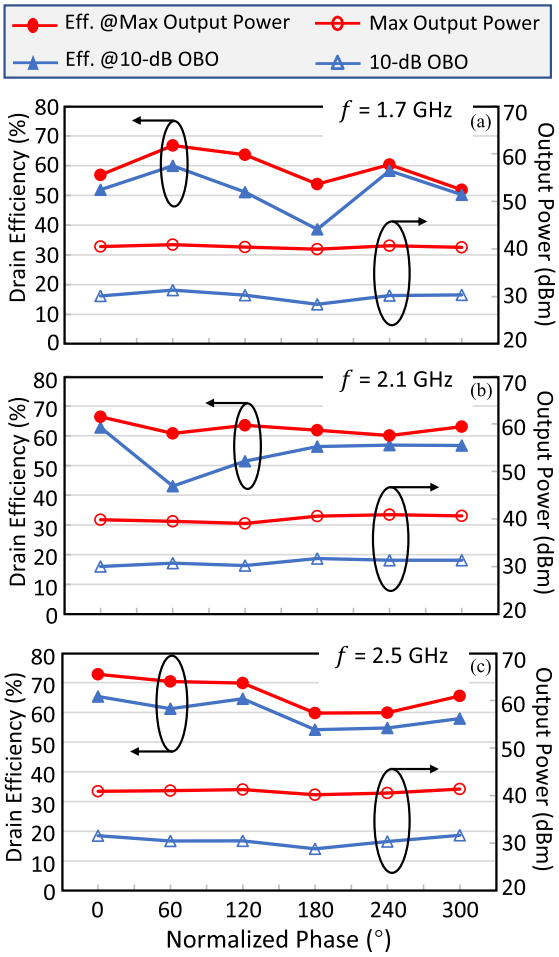

Fig. 21. Measured DE and output power over 2:1 VSWR with CW signal at (a) 1.7 GHz, (b) 2.1 GHz, (c) 2.5 GHz.

B. Modulated Measurement

In order to validate the linearity of the proposed circuit under realistic communication conditions, the modulated measurement is presented with a 20 MHz modulation-bandwidth single-carrier 64 QAM LTE signal at three in-band frequency 1.7, 2.1, and 2.5 GHz. The measurement was first performed under matched conditions. Fig. 22 shows the measured power spectral density (PSD) under matched condition, the ACPR of most measured frequencies are higher than 20 dB without any digital predistortion. Fig. 23 shows the proposed PD-LMBA achieves the average drain efficiency (DE) of 56.4%–62% and average output power of 30.9–31.5 dBm over the designed frequency band.

The proposed PD-LMBA is further measured under the 2:1 VSWR load mismatch to present the mismatch-resilient feature. Fig. 23 shows the optimal results obtained with six phase mismatch load over VSWR 2:1 circle, it achieves average drain efficiency of 44.7%–53.5% with the average output power of 29.8%–30.6% dBm at 1.7 GHz, average drain efficiency of 52.1%–59.1% with the average output power of 30–31.3 dBm at 2.1 GHz and average drain efficiency of 45.5%-55% with the average output power of 29–30.8 dBm at 2.5 GHz.

TABLE II
COMPARISON WITH STATE-OF-THE-ART OF RECENTLY REPORTED MISMATCH-RESILIENT PAS

Ref./ Year	This Work				[30] TMTT-2021		[33] TMTT-2021		[34] TMTT-2021		[31] TMTT-2022		[48] TMT[T-2022	
Technology	GaN-PCB				GaN-PCB		GaN-PCB*		LDMOS-PCB		GaN-PCB		GaN-PCB*	
Freq (GHz)	1.7 — 2.9				3.5		3.55		0.9		1.7 — 2.7		3.6	
Control Variables	1-D				3-D		1-D (No load modulation)		2-D		3-D		4-D	
Load (Z_0/VSWR)	50 Ω	2:1 VSWR @1.7GHz	2:1 VSWR @2.1GHz	2:1 VSWR @2.5GHz	50 Ω	2:1	50 Ω	2:1	50 Ω	2:1	50 Ω	2:1	50 Ω	2:1
P_{Max} (dBm)	39.4-43.1	39.9-40.9	39.1-40.9	40.2-41.4	42*	-	40.3*	37.3	29.4	29.4	40.1-41.8	39.1-41	43.5	42
DE_{Max} (%)	65.3-76.9	51.9-66.8	60.1-66.4	59.8-72.8	63.5-70.1	-	65*	-	59.1	46.5-51.3	56 - 78	-	64*	58
DE@10dB OBO(%)	54.5-70.5	38.6-59.9	43.0-62.8	54.2-65.4	34*-36*	-	-	-	25*	18*- 30*	30 - 57*	-	32*	27*- 35*
Modulation Signal	64-QAM 20 MHz				64-QAM 20 MHz		OFDM 20 MHz		64-QAM 3.86 MHz		64-QAM 20 MHz		LTE 5 MHZ	
$P_{OUT,avg}$ (dBm) / DE_{avg} (%)	30.9-31.5 / 56.4-62.0	29.8-30.6 / 44.7-53.5	30-31.3 / 52.1-59.1	29-30.8 / 45.5-55.0	37.2 / 47.3	33-34.2 / 32.5-42.5	33.5* / 25.3*	-	22 / 24.4	22 / 21-23	33.1-33.7 / 41.3-44.6	33.1 / 42.9	43.5 / 46.4	42* / 43

* Graphically estimated

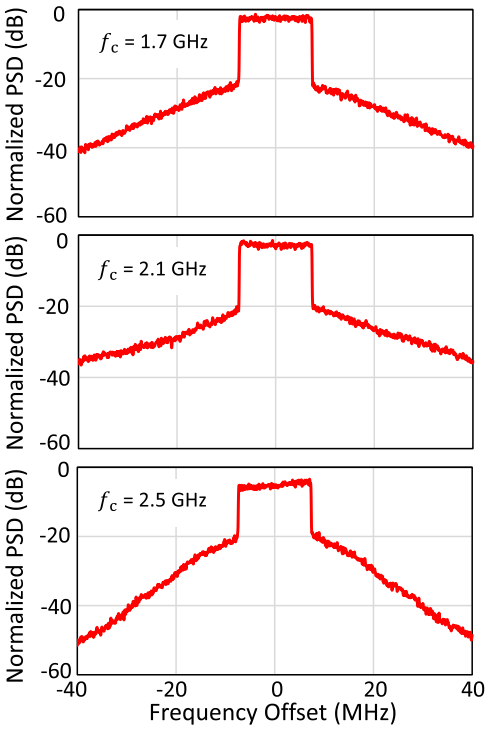

Fig. 22. Modulation signal measurement over 1.7–2.5 GHz at matched-load condition.

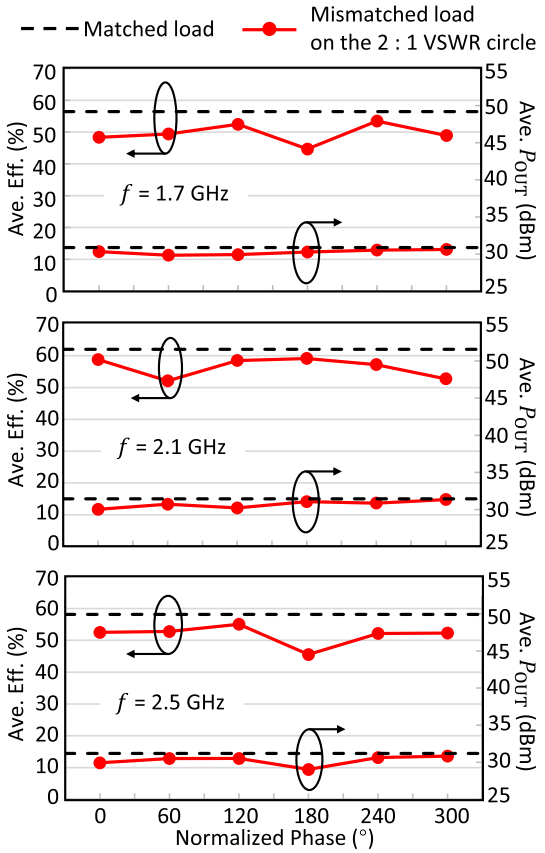

Fig. 23. Modulation signal measurement over 1.7–2.5 GHz under mismatch.

The PD-LMBA is intrinsically nonlinear due to the over-driving of CA, which leads to the high ACLR. There are multiple ways to mitigate this CA over-driving issue, such as digital-assisted dual-input design [42] and equipping CA with load modulation through asymmetrical biasing of BA [37], [43]. Moreover, DPD has been successfully applied to LMBA in literature. Together with the recent advances in load-mismatch tolerable DPD [44] and array-level DPD [45], [46], [47], the presented 1-D reconfigurable PD-LMBA can be effectively linearized in both matched and mismatched conditions which leads to a further research topic of enhancing the performance of PD-LMBA.

A comprehensive comparison between the proposed PD-LMBA and other recently announced mismatch-resilient PAs is shown in Table II. It is important to emphasize that the first ever 1-D reconfiguration operation under mismatch is accomplished with a very competitive profile. Specifically, an overall wider operation bandwidth is implemented in either match or mismatch condition. Moreover, the proposed PD-LMBA indicates a higher maximum DE at maximum power output. Additionally, compared with the designs in [48] and [34], this work presents a great promotion of DE at 10-dB OBO level. Using the same modulation bandwidth signal in [30], this circuit exhibits larger average DE and output power. Therefore, The proposed PD-LMBA clearly exhibits better

mismatch resilience and well validates the effectiveness of the proposed theory.

VI. Conclusion

This article introduces a novel 1-D reconfiguration PD-LMBA with coincidental wide bandwidth operation and mismatch resilience for the first time. Through comprehensive theoretical analysis, the BA in PD-LMBA inherits the VSWR insensitivity of balanced amplifiers, which is in coordination with the 1-D reconfiguration of the carrier amplifier by setting load-dependent voltage ($V_{\mathrm{DD,CA}}$). The proposed circuit is verified through an emulated model, proving that the peaking amplifiers (BA1 and BA2) have load impedance dependence and can accompany each other given the condition that CA (once saturated) features a duality between CS and VS. As a result, the overall efficiency of PD-LMBA can be maintained under mismatch condition. To experimentally validate the proposed theory, a prototype is developed, and the measured results show that the designed PD-LMBA exhibits a highly efficient performance over the target 1.7–2.9 bandwidth at both 10-dB back-off and peak power. With the 1-D reconfiguration of $V_{\mathrm{DD,CA}}$, the efficiency performance is experimentally maintained under 2:1 VSWR of load mismatch at in-band frequencies of 1.7, 2.1 and 2.5 GHz, offering up to 72.8% of efficiency at peak power while delivering 38.6–65.4% efficiency at all back-off levels down to 10-dB OBO. The proposed technology can offer maximized efficiency and minimized system complexity against arbitrary load mismatch, and it clearly exhibits a promising potential for application to next-generation array-based massive MIMO communication systems.

Appendix

In Section II, the analytical load-modulation behaviors of CA and BA with respect to z_{L} are derived based on an identical current BA1 and BA2, I_b. However, the actual circuit using emulated model shows different currents of BA1 and BA2 in simulation. For the readers' reference, the equations are re-derived based on different I_{b1} and I_{b2} as follows:

$$z_{\mathrm{BA1}} = \frac{\sqrt{2}I_c}{I_{b1}} + \frac{I_{b2}}{I_{b1}}, \quad z_{\mathrm{BA2}} = \frac{\sqrt{2}I_c}{z_{\mathrm{L}}I_{b2}} + \frac{2}{z_{\mathrm{L}}} - \frac{I_{b1}}{I_{b2}} \tag{21}$$

$$z_{\mathrm{CA}} = \frac{1}{z_{\mathrm{L}}} + \frac{\sqrt{2}(I_{b2} - z_{\mathrm{L}}I_{b1})}{z_{\mathrm{L}}I_c}. \tag{22}$$

It is important to note that the asymmetry between I_{b1} and I_{b2} consistently supports the discussions of mismatch-resilient load modulation of PD-LMBA in Section III-C.

References

[1] N. Kumari, S.-H. Yang, K.-H. Chen, Y.-H. Lin, S.-R. Lin, and T.-Y. Tsai, "A CMOS switched-capacitor boost mode envelope tracking regulator with 4% efficiency improvement at 7.7dB PAPR for 20MHz LTE envelope tracking RF power amplifiers," in *Proc. IEEE Asian Solid-State Circuits Conf. (A-SSCC)*, Nov. 2019, pp. 255–258.

[2] K. Hamano, H. Shimizu, and K. Nishikawa, "Analysis of phase offset impact on millimeter-wave broadband Doherty amplifier MMIC," in *Proc. IEEE Int. Symp. Radio-Frequency Integr. Technol. (RFIT)*, Aug. 2021, pp. 1–3.

[3] L. Lin, L. Yang, S. Zheng, and J. Peng, "A 10W fully-integrated LDMOS MMIC Doherty in LGA package for 2.7GHz small cell application," in *IEEE MTT-S Int. Microw. Symp. Dig.*, Jun. 2019, pp. 1434–1437.

[4] H. T. Nguyen and H. Wang, "A coupler-based differential Doherty power amplifier with built-in baluns for high mm-wave linear-yet-efficient Gbit/s amplifications," in *Proc. IEEE Radio Freq. Integr. Circuits Symp. (RFIC)*, Jun. 2019, pp. 195–198.

[5] Y. Zhao, X. Li, C. Gai, X. Du, M. Helaoui, and F. Ghannouchi, "Optimal fundamental load modulation for class-X harmonically tuned power amplifier," in *Proc. IEEE Asia–Pacific Microw. Conf. (APMC)*, Dec. 2019, pp. 1649–1651.

[6] W. Lim et al., "Dual-mode CMOS power amplifier based on load-impedance modulation," *IEEE Microw. Wireless Compon. Lett.*, vol. 28, no. 11, pp. 1041–1043, Nov. 2018.

[7] Y. Cao and K. Chen, "Pseudo-Doherty load-modulated balanced amplifier with wide bandwidth and extended power back-off range," *IEEE Trans. Microw. Theory Techn.*, vol. 68, no. 7, pp. 3172–3183, Jul. 2020.

[8] D. J. Shepphard, J. Powell, and S. C. Cripps, "An efficient broadband reconfigurable power amplifier using active load modulation," *IEEE Microw. Wireless Compon. Lett.*, vol. 26, no. 6, pp. 443–445, Jun. 2016.

[9] E. R. Srinidhi et al., "Digitally assisted load modulated balanced amplifier for 200W cellular infrastructure applications," in *IEEE MTT-S Int. Microw. Symp. Dig.*, Aug. 2020, pp. 719–722.

[10] T. Cappello, P. H. Pednekar, C. Florian, Z. Popovic, and T. W. Barton, "Supply modulation of a broadband load modulated balanced amplifier," in *IEEE MTT-S Int. Microw. Symp. Dig.*, Jun. 2018, pp. 304–307.

[11] C. R. Chappidi, T. Sharma, Z. Liu, and K. Sengupta, "Load modulated balanced mm-wave CMOS PA with integrated linearity enhancement for 5G applications," in *IEEE MTT-S Int. Microw. Symp. Dig.*, Aug. 2020, pp. 1101–1104.

[12] K. Vivien, P. E. de Falco, G. Baudoin, O. Venard, P. P. C. Felix, and T. Barton, "Load modulated balanced amplifier designed for AM-PM linearity," in *Proc. 50th Eur. Microw. Conf. (EuMC)*, Jan. 2021, pp. 304–307.

[13] P. H. Pednekar and T. W. Barton, "RF-input load modulated balanced amplifier," in *IEEE MTT-S Int. Microw. Symp. Dig.*, Jun. 2017, pp. 1730–1733.

[14] P. H. Pednekar, E. Berry, and T. W. Barton, "RF-input load modulated balanced amplifier with octave bandwidth," *IEEE Trans. Microw. Theory Techn.*, vol. 65, no. 12, pp. 5181–5191, Dec. 2017.

[15] R. Quaglia and S. Cripps, "A load modulated balanced amplifier for telecom applications," *IEEE Trans. Microw. Theory Techn.*, vol. 66, no. 3, pp. 1328–1338, Mar. 2018.

[16] J. Pang, C. Chu, Y. Li, and A. Zhu, "Broadband RF-input continuous-mode load-modulated balanced power amplifier with input phase adjustment," *IEEE Trans. Microw. Theory Techn.*, vol. 68, no. 10, pp. 4466–4478, Oct. 2020.

[17] Y. Cao, H. Lyu, and K. Chen, "Asymmetrical load modulated balanced amplifier with continuum of modulation ratio and dual-octave bandwidth," *IEEE Trans. Microw. Theory Techn.*, vol. 69, no. 1, pp. 682–696, Jan. 2021.

[18] Y. Cao and K. Chen, "Hybrid asymmetrical load modulated balanced amplifier with wide bandwidth and three-way-Doherty efficiency enhancement," *IEEE Microw. Wireless Compon. Lett.*, vol. 31, no. 6, pp. 721–724, Jun. 2021.

[19] T. L. Marzetta, *Fundamentals Massive MIMO*. Cambridge, U.K.: Cambridge Univ. Press, 2016.

[20] L. Savy and M. Lesturgie, "Coupling effects in MIMO phased array," in *Proc. IEEE Radar Conf. (RadarConf)*, May 2016, pp. 1–6.

[21] C. Fager, T. Eriksson, F. Barradas, K. Hausmair, T. Cunha, and J. C. Pedro, "Linearity and efficiency in 5G transmitters: New techniques for analyzing efficiency, linearity, and linearization in a 5G active antenna transmitter context," *IEEE Microw. Mag.*, vol. 20, no. 5, pp. 35–49, May 2019.

[22] K.-H. Chen and J.-F. Kiang, "Effect of mutual coupling on the channel capacity of MIMO systems," *IEEE Trans. Veh. Technol.*, vol. 65, no. 1, pp. 398–403, Jan. 2016.

[23] X. Chen, S. Zhang, and Q. Li, "A review of mutual coupling in MIMO systems," *IEEE Access*, vol. 6, pp. 24706–24719, 2018.

[24] M. Gilasgar, A. Barlabe, and L. Pradell, "A 2.4 GHz CMOS class-F power amplifier with reconfigurable load-impedance matching," *IEEE Trans. Circuits Syst. I, Reg. Papers*, vol. 66, no. 1, pp. 31–42, Jan. 2019.

[25] J. Chen, X. Meng, M. Zhou, and Y. Jin, "Bonding wire based RF front-end tunable impedance matching network for K and Ka bands," in *Proc. Cross Strait Radio Sci. Wireless Technol. Conf. (CSRSWTC)*, Oct. 2021, pp. 313–315.

[26] Y.-C. Lee and J.-S. Fu, "A 5.8-GHz power amplifier with an on-chip tunable output matching network," in *Proc. Asia–Pacific Microw. Conf.*, 2011, pp. 219–222.
[27] F. Ziraksaz and A. Hassanzadeh, "A 23.4–31.9 GHz tunable RF-MEMS impedance matching network for 5G power amplifier," in *Proc. 29th Iranian Conf. Electr. Eng. (ICEE)*, May 2021, pp. 69–73.
[28] N. S. Mannem, M.-Y. Huang, T.-Y. Huang, and H. Wang, "A reconfigurable hybrid series/parallel Doherty power amplifier with antenna VSWR resilient performance for MIMO arrays," *IEEE J. Solid-State Circuits*, vol. 55, no. 12, pp. 3335–3348, Dec. 2020.
[29] H. Lyu and K. Chen, "Balanced-to-Doherty mode-reconfigurable power amplifier with high efficiency and linearity against load mismatch," *IEEE Trans. Microw. Theory Techn.*, vol. 68, no. 5, pp. 1717–1728, May 2020.
[30] H. Lyu, Y. Cao, and K. Chen, "Linearity-enhanced quasi-balanced Doherty power amplifier with mismatch resilience through series/parallel reconfiguration for massive MIMO," *IEEE Trans. Microw. Theory Techn.*, vol. 69, no. 4, pp. 2319–2335, Apr. 2021.
[31] H. Lyu and K. Chen, "Analysis and design of reconfigurable multiband mismatch-resilient quasi-balanced Doherty power amplifier for massive MIMO systems," *IEEE Trans. Microw. Theory Techn.*, vol. 70, no. 10, pp. 4410–4421, Oct. 2022.
[32] C. R. Chappidi, T. Sharma, and K. Sengupta, "Multi-port active load pulling for mm-wave 5G power amplifiers: Bandwidth, back-off efficiency, and VSWR tolerance," *IEEE Trans. Microw. Theory Techn.*, vol. 68, no. 7, pp. 2998–3016, Jul. 2020.
[33] C. F. Gonçalves, F. M. Barradas, L. C. Nunes, P. M. Cabral, and J. C. Pedro, "Dynamic supply voltage control for PA output power correction under variable loading scenarios," *IEEE Trans. Microw. Theory Techn.*, vol. 69, no. 1, pp. 745–755, Jan. 2021.
[34] G. D. Singh, H. M. Nemati, and L. C. N. de Vreede, "A low-loss load correction technique for self-healing power amplifiers using a modified two-tap six-port network," *IEEE Trans. Microw. Theory Techn.*, vol. 69, no. 9, pp. 4069–4081, Sep. 2021.
[35] S. Probst, L. Berkelmann, B. Luers, B. Geck, and D. Manteuffel, "Investigation of the dynamic load modulation of an inverse class-F power amplifier with an adaptive matching network," in *Proc. IEEE Topical Conf. RF/Microw. Power Modeling Radio Wireless Appl. (PAWR)*, Jan. 2018, pp. 20–22.
[36] S. C. Cripps, "RF power amplifiers for wireless communications," *IEEE Microw. Mag.*, vol. 1, no. 1, p. 64, Mar. 2000.
[37] Y. Cao, H. Lyu, and K. Chen, "Continuous-mode hybrid asymmetrical load-modulated balanced amplifier with three-way modulation and multi-band reconfigurability," *IEEE Trans. Circuits Syst. I, Reg. Papers*, vol. 69, no. 3, pp. 1077–1090, Mar. 2022.
[38] M. Muraguchi, T. Yukitake, and Y. Naito, "Optimum design of 3-Db branch-line couplers using microstrip lines," *IEEE Trans. Microw. Theory Techn.*, vol. MTT-31, no. 8, pp. 674–678, Aug. 1983.
[39] K. Chen and D. Peroulis, "Design of highly efficient broadband class-E power amplifier using synthesized low-pass matching networks," *IEEE Trans. Microw. Theory Techn.*, vol. 59, no. 12, pp. 3162–3173, Dec. 2011.
[40] Y. Cao, H. Lyu, and K. Chen, "Load modulated balanced amplifier with reconfigurable phase control for extended dynamic range," in *IEEE MTT-S Int. Microw. Symp. Dig.*, Jun. 2019, pp. 1335–1338.
[41] Y. Cao and K. Chen, "Dual-octave-bandwidth RF-input pseudo-Doherty load modulated balanced amplifier with $\geq$ 10-dB power back-off range," in *IEEE MTT-S Int. Microw. Symp. Dig.*, Aug. 2020, pp. 703–706.
[42] K. Chaudhry, R. Quaglia, and S. Cripps, "A load modulated balanced amplifier with linear gain response and wide high-efficiency output power back-off region," in *Proc. Int. Workshop Integr. Nonlinear Microw. Millimetre-Wave Circuits (INMMiC)*, Jul. 2020, pp. 1–3.
[43] Y. Cao, H. Lyu, and K. Chen, "Asymmetrical load modulated balanced amplifier with continuum of modulation ratio and dual-octave bandwidth," *IEEE Trans. Microw. Theory Techn.*, vol. 69, no. 1, pp. 682–696, Jan. 2021.
[44] X. Wang, Y. Li, and A. Zhu, "Digital predistortion using extended magnitude-selective affine functions for 5G handset power amplifiers with load mismatch," *IEEE Trans. Microw. Theory Techn.*, vol. 70, no. 5, pp. 2825–2834, May 2022.
[45] X. Wang, Y. Li, C. Yu, W. Hong, and A. Zhu, "Digital predistortion of 5G massive MIMO wireless transmitters based on indirect identification of power amplifier behavior with OTA tests," *IEEE Trans. Microw. Theory Techn.*, vol. 68, no. 1, pp. 316–328, Jan. 2020.
[46] X. Liu, W. Chen, L. Chen, F. M. Ghannouchi, and Z. Feng, "Linearization for hybrid beamforming array utilizing embedded over-the-air diversity feedbacks," *IEEE Trans. Microw. Theory Techn.*, vol. 67, no. 12, pp. 5235–5248, Dec. 2019.
[47] E. Ng, Y. Beltagy, G. Scarlato, A. Ben Ayed, P. Mitran, and S. Boumaiza, "Digital predistortion of millimeter-wave RF beamforming arrays using low number of steering angle-dependent coefficient sets," *IEEE Trans. Microw. Theory Techn.*, vol. 67, no. 11, pp. 4479–4492, Nov. 2019.
[48] C. F. Goncalves, F. M. Barradas, L. C. Nunes, P. M. Cabral, and J. C. Pedro, "Quasi-load insensitive Doherty PA using supply voltage and input excitation adaptation," *IEEE Trans. Microw. Theory Techn.*, vol. 70, no. 1, pp. 779–789, Jan. 2022.

Jiachen Guo (Student Member, IEEE) received the M.S. degree in computer engineering from the Syracuse University, Syracuse, NY, USA, in 2021. He is currently pursuing the Ph.D. degree in electrical engineering at the University of Central Florida, Orlando, FL, USA.

His research interests include novel highly efficient broadband and linear PA architectures and reconfigurable RF/millimeter-wave circuits design.

Dr. Guo was a recipient of the Second Place Award of the Student Design Competition on High Efficiency Power Amplifier at IEEE MTT-S IMS in 2020.

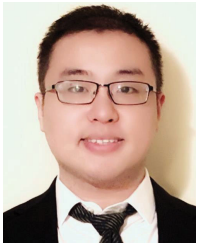

Yuchen Cao (Member, IEEE) received the bachelor's degree in engineering from Zhejiang University, Hangzhou, Zhejiang, China, in 2011, the master's degree from Wichita State University, Wichita, KS, USA, in 2016, and the Ph.D. degree in electrical engineering from the University of Central Florida, Orlando, FL, USA, in 2022.

He is currently a Senior Design Engineer with Qorvo, Inc., Apopka, FL, USA. His research interests include highly efficient broadband PAs, BAW filters, integrated RF front-ends, carrier aggregation, and millimeter-wave circuit design.

Dr. Cao was a recipient of the First Place Award of the Student Paper Competition, in the IEEE Microwave Theory and Techniques Society (IEEE MTT-S) International Microwave Symposium (IMS) in 2020, the First Place Award of the Student Design Competition on High Efficiency Power Amplifier in IEEE MTT-S IMS in 2020 and 2021, respectively, the First Place Award of the Student Design Competition on Carrier Aggregation BAW Quadplexer Module in IEEE MTT-S IMS, in 2018 and 2019, respectively, and the Second Place Award of Student Paper Competition in IEEE WAMICON 2019. He served as the IEEE MTT-S/AP-S Orlando Chapter Chair in 2021–2022. He has been a Reviewer for the IEEE TRANSACTIONS ON MICROWAVE THEORY AND TECHNIQUES and the IEEE TRANSACTIONS ON CIRCUITS AND SYSTEM—I.

Kenle Chen (Senior Member, IEEE) received the bachelor's degree in communication engineering from Xi'an Jiaotong University, Xi'an, Shaanxi, China, in 2005, the master's degree in electronics and information engineering from Peking University, Beijing, China, in 2008, and the Ph.D. degree in electrical engineering from Purdue University, West Lafayette, IN, USA, in 2013.

He is currently an Assistant Professor with the Department of Electrical and Computer Engineering, University of Central Florida, Orlando, FL, USA. His research interests include energy-efficient, wideband, and ultrahigh-speed RF/mm-Wave circuits and systems for 5G-and-beyond communications, extreme-performance PAs in CMOS and compound semiconductor technologies, reconfigurable RF/mm-Wave electronics, and innovational wireless radio concepts/architectures/applications. Prior to his career in academia, he has extensive experience in wireless and semiconductor industries. From 2015 to 2017, he worked as a Staff RFIC Engineer with Skyworks Solutions, Inc., Irvine, CA, USA, where he focused on the development of RF frontend modules for the advanced Smart-Phone platforms. From 2013 to 2015, he worked as a Principal/Lead RFIC Engineer with innovational startups, where he led the Research and Development of multiple successful products of CMOS integrated PAs and frontend solutions for the latest WLAN platforms, e.g., IEEE802.11ac/ax.

Dr. Chen was a recipient of the 2012 IEEE Microwave Theory and Techniques Society (MTT-S) Graduate Fellowship. He is an Associate Editor of the IEEE TRANSACTIONS ON MICROWAVE THEORY AND TECHNIQUES.